

## 1                                      **Activation of cGAS/STING pathway upon paramyxovirus infection**

2  
3 Mathieu Iampietro<sup>1\*</sup>, Claire Dumont<sup>1</sup>, Cyrille Mathieu<sup>1</sup>, Julia Spanier<sup>2</sup>, Jonathan Robert<sup>1</sup>, Aude  
4 Charpenay<sup>1</sup>, Sébastien Dupichaud<sup>1</sup>, Kevin P. Dhondt<sup>1</sup>, Noémie Aurine<sup>1</sup>, Rodolphe Pelissier<sup>1</sup>, Marion  
5 Ferren<sup>1</sup>, Stéphane Mély<sup>3</sup>, Denis Gerlier<sup>1</sup>, Ulrich Kalinke<sup>2,4</sup> and Branka Horvat<sup>1\*</sup>  
6

### 7 **Author's affiliation:**

8 <sup>1</sup> CIRI, Centre International de Recherche en Infectiologie, INSERM U1111, CNRS, UMR5308, Univ  
9 Lyon, Université Claude Bernard Lyon 1, École Normale Supérieure de Lyon, France.

10 <sup>2</sup> Institute for Experimental Infection Research, TWINCORE, Centre for Experimental and Clinical  
11 Infection research, a joint venture between the Hanover Medical School and the Helmholtz Centre  
12 for Infection Research, Hanover, Germany.

13 <sup>3</sup> INSERM- Laboratoire P4 Jean Mérieux-21 Avenue Tony Garnier, 69365 Lyon, France.

14 <sup>4</sup> Cluster of Excellence-Resolving Infection Susceptibility (RESIST), Hanover, Germany.

15  
16 **\*Correspondence:** Mathieu Iampietro ([mathieu.iampietro@inserm.fr](mailto:mathieu.iampietro@inserm.fr)) and Branka Horvat  
17 ([branka.horvat@inserm.fr](mailto:branka.horvat@inserm.fr)), Centre International de Recherche en Infectiologie (CIRI), INSERM  
18 U1111, 21 Avenue Tony Garnier, 69007, Lyon, France  
19  
20  
21

### 22 **SUMMARY**

23             During inflammatory diseases, cancer and infection, the cGAS/STING pathway is known to  
24 recognize foreign or self-DNA in the cytosol and activate an innate immune response. Here, we  
25 report that negative-strand RNA paramyxoviruses, Nipah virus (NiV) and Measles virus (MeV),  
26 can also trigger the cGAS/STING axis. While mice deficient for MyD88, TRIF and MAVS still  
27 moderately control NiV infection when compared to WT mice, additional STING deficiency  
28 resulted in 100% lethality, suggesting synergistic roles of these pathways in host protection.  
29 Moreover, deletion of cGAS or STING resulted in decreased type-I interferon production with  
30 enhanced paramyxoviral infection in both human and murine cells. Finally, the phosphorylation  
31 and ubiquitination of STING, observed during viral infections, confirmed the activation of  
32 cGAS/STING pathway by NiV and MeV. Our data suggest that cGAS/STING activation is critical in  
33 controlling paramyxovirus infection, and possibly represent attractive targets to develop  
34 countermeasures against severe disease induced by these pathogens.  
35

36 **Keywords:** (10 max): Paramyxovirus, Nipah virus, Measles virus, cGAS, STING, emerging infection,  
37 innate immunity, inflammatory response, phosphorylation, ubiquitination  
38

### 39 **INTRODUCTION**

40             The innate immunity represents the first line of host defense against invading pathogens  
41 (Akira et al., 2006). Exogenous motifs associated with viral infections involved in stimulating innate  
42 responses include pathogen-derived nucleic acids, DNA or RNA (Akira et al., 2006; Mogensen, 2009).  
43 Its ensuing detection activates pattern recognition receptor (PRR)-associated adaptor molecules  
44 that are responsible for subsequent expression of type I and III interferons (IFNs) (Park and Iwasaki,  
45 2020) and the induction of IFN-related genes, which are important for the control of virus infection  
46 (Borden et al., 2007; Der et al., 1998; Sen and Peters, 2007). Four major axes, defined by their nodal  
47 adaptor, are able to induce strong innate immune responses upon sensing of pathogen-related  
48 nucleic acids (Baccala et al., 2009). Three of them, Toll-like receptor (TLR)-associated adaptor  
49 molecules: myeloid differentiation primary response 88 (MyD88) (Wesche et al., 1997),

50 Toll/interleukin-1 receptor/resistance [TIR] domain-containing adaptor-inducing IFN- $\beta$  (TRIF)  
51 (Yamamoto et al., 2003) and RIG-I-like receptor (RLR)-associated mitochondrial antiviral signaling  
52 protein (MAVS) (Seth et al., 2005) are dedicated to sense DNA and/or RNA. The cyclic guanosine  
53 monophosphate-adenosine monophosphate (cGAMP) synthase (cGAS)/stimulator of interferon  
54 genes (STING also known as ERIS, MITA or TMEM173) pathway is the leading sensor for the  
55 detection of cytosolic DNA (Ishikawa and Barber, 2008; Sun et al., 2013). The cGAS/STING axis seems  
56 to be involved in the sensing of various different RNA viruses, which may express viral proteins that  
57 counteract cGAS/STING activity at different levels. Thus, the cGAS/STING pathway may also  
58 contribute to the control of RNA viruses (Ni et al., 2018). Recently, activation of the cGAS/STING  
59 pathway has been observed following infection by the positive strand RNA virus SARS-CoV-2  
60 (Neufeldt et al., 2020).

61 In recent years, members of the *Paramyxoviridae* family have caused numerous emerging  
62 zoonoses and/or epidemics (Thibault et al., 2017). This viral family contains both old and new human  
63 and zoonotic viral pathogens such as measles virus (MeV) and Nipah virus (NiV). While MeV has  
64 been almost eradicated from most developed countries through vaccination campaigns, the  
65 number of cases and deaths significantly increased within the last decade killing more than 100.000  
66 people every year (Ferren et al., 2019). Moreover, as NiV is the most virulent paramyxovirus with  
67 mortality rates between 40-100% during epidemics and remains without any licensed treatment or  
68 vaccine (Pelissier et al., 2019; Soman Pillai et al., 2020), the World Health Organization included it  
69 in its blueprint for priority pathogens (Mehand et al., 2018).

70 Our previous work evaluating innate sensors involved in the protection of mice following NiV  
71 infection suggests control of the virus through the activation of MyD88 and MAVS pathways, while  
72 TRIF seems dispensable (Iampietro et al., 2020). Although, both MyD88 and MAVS are important to  
73 produce high levels of type-I IFNs (IFN-I), double KO mice still exhibit some resistance against NiV  
74 infection. This is in contrast to the interferon- $\alpha/\beta$  receptor (IFNAR) KO mice that lack any IFN-I-  
75 related responses and are unable to control NiV infection (Dhondt et al., 2013; Iampietro et al.,  
76 2020). We thus hypothesized that the cGAS/STING axis of the innate immunity could also contribute  
77 to the control of NiV infection.

78 Once activated in the cytoplasm of infected cells, cGAS uses adenosine triphosphate (ATP)  
79 and guanosine triphosphate (GTP) as substrates for cyclisation into cGAMP. cGAMP triggers STING  
80 and further results in IFN-I expression (Ishikawa and Barber, 2008; Sun et al., 2013). Successive  
81 conformational changes ensure the activation of cGAS and STING in cascade. Briefly, cGAS in  
82 "resting" state is a monomer containing a conserved zinc-ion-binding domain as DNA binding  
83 module (Civril et al., 2013; Kranzusch et al., 2014). Upon DNA binding in the cytoplasm, cGAS  
84 dimerizes and further oligomerizes to induce optimal cGAMP production (Gao et al., 2013; Zhang et  
85 al., 2014). Thereafter, cGAMP binds to STING in its ligand-binding domain and induces inward  
86 rotations leading to dimerization and later oligomerization of STING (Cong et al., 2019; Ergun et al.,  
87 2019; Shang et al., 2012). In addition, upon binding of cGAMP, STING exits the endoplasmic  
88 reticulum to the Golgi apparatus. There, it transduces a downstream signaling pathway by recruiting  
89 TANK-binding kinase 1 (TBK1) and IRF-3 (but not IRF-7) transactivator and activating the NF- $\kappa$ B  
90 pathway that results in the activation of type I IFN and cytokine genes (Dobbs et al., 2015; Gui et  
91 al., 2019; Liu et al., 2015). The recruitment of IRF-3 relies on the phosphorylation of its Ser366  
92 (Ser365 in murine) STING by TBK1 (Tsuchiya et al., 2016). In addition, the E3 ubiquitin ligases TRIM32  
93 and TRIM56 promotes the non-degradative K-63 linked ubiquitination of Lys224 of STING to trigger  
94 a cytokine response (Ni et al., 2017; Tanaka and Chen, 2012). As a third type of post-translational  
95 modifications (PTMs) STING palmitoylation governs its trafficking to the Golgi (Mukai et al., 2016).

96 We report here that both cGAS and STING are required for mounting an efficient innate  
97 immune response upon NiV and MeV infection. In infected cells, STING is phosphorylated on S366  
98 (S365 in mouse) and is K63 linked ubiquitinated, confirming the presence of its activated form at

99 later time points of RNA virus infection, similarly to what has been observed by others after infection  
100 with DNA virus (Chiang and Gack, 2017).

101

## 102 RESULTS

103

### 104 **STING plays a role in the control of NiV infection in mice.**

105 Our previous study revealed a complementary role of MyD88 and MAVS in the partial  
106 containment of NiV, suggesting that the complete resistance of mice against NiV involves an  
107 additional activation pathway of the IFN-I response (Iampietro et al., 2020). The cGAS/STING axis  
108 has recently emerged as critical in the crosstalk between innate sensing of cytosolic DNA and RNA  
109 viruses (Ni et al., 2018). We therefore analyzed the susceptibility of mice bearing gene deletions in  
110 either single TLR and IL-1R (MyD88 KO) pathway, or in combination with TRIF (MyD88/TRIF KO),  
111 MAVS (MyD88/TRIF/MAVS KO) and STING (MyD88/TRIF/MAVS/STING KO) signaling platforms  
112 (**Figure 1 and S1**). The animals were infected intraperitoneally and monitored during 24 days for  
113 clinical signs and/or death. While infected wild-type (WT) mice, MyD88 KO and MyD88/TRIF KO mice  
114 did not manifest any clinical signs of disease, triple MyD88/TRIF/MAVS KO and quadruple  
115 MyD88/TRIF/MAVS/STING KO mice exhibited symptoms of neurological disorders similar to those  
116 observed in IFNAR KO mice (**Figure 1A**). Moreover, while 60% triple KO mice survived NiV challenge,  
117 all mice bearing the quadruple deficiency succumbed by day 11 post-infection, indicating a crucial  
118 and non-redundant role for STING in the protection of mice (**Figure 1A**). NiV nucleoprotein (NiV-N)  
119 protein levels in the brain of autopsied animals deficient for MyD88/TRIF/MAVS and  
120 MyD88/TRIF/MAVS/STING were comparable to those observed in the brain of IFNAR KO mice at  
121 time of death (**Figure 1B**). Furthermore, while analysis of NiV load in murine brain determined  
122 equivalent NiV-N RNA levels within these three deficient murine models, evaluation in the spleen  
123 showed higher viral loads in mice bearing the quadruple deficiency compared to the triple KO mice  
124 (**Figure 1C and S1A**). In parallel, the lower production of IFN $\beta$  (**Figure 1D and S1B**) and IFN $\alpha$  (**Figure**  
125 **1E and S1C**) in the brains and spleens of MyD88/TRIF/MAVS KO and MyD88/TRIF/MAVS/STING KO  
126 mice compared to WT was associated with their inability to clear the virus. Overall, these results  
127 confirm our previous observations on the importance of the RLR signaling platform involving MAVS  
128 (Iampietro et al., 2020) and suggest a novel synergistic and non-redundant role of the STING  
129 pathway during NiV infection.

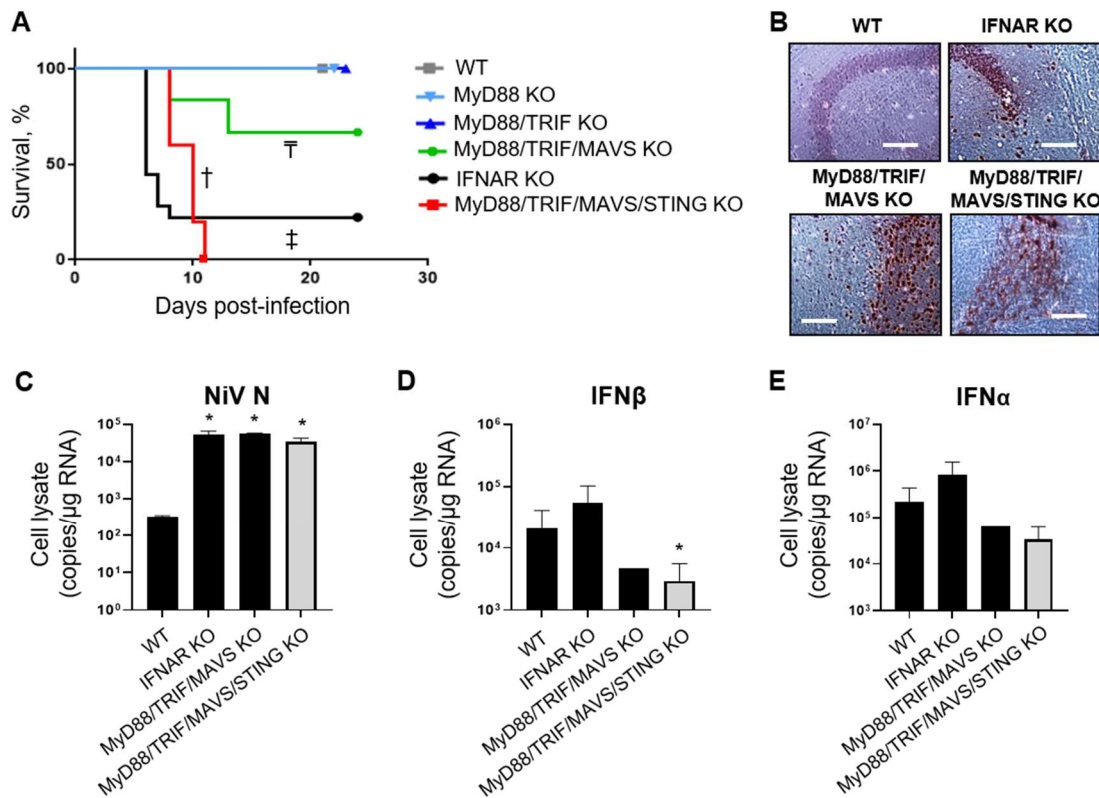
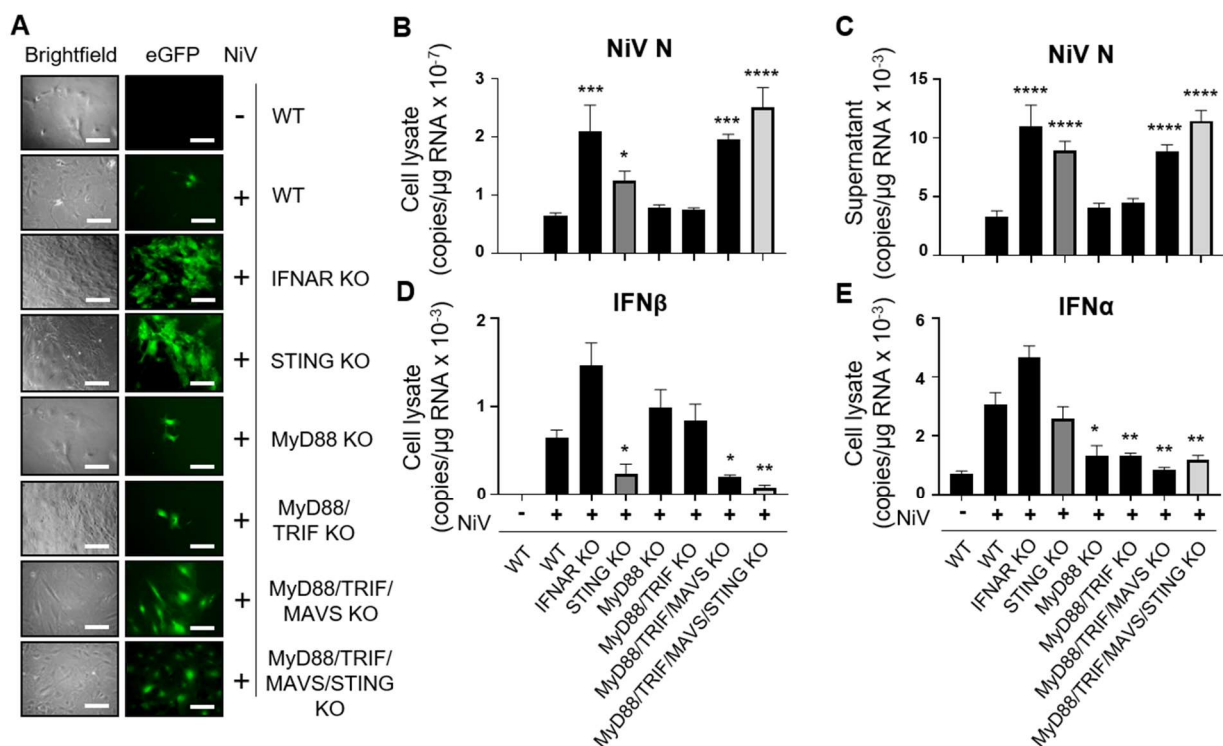


**Figure 1. STING plays a role in the control of NiV infection in mice.** Wild-type (WT) mice and mice deficient in indicated pathogen recognition signaling pathways were infected intraperitoneally with 10<sup>6</sup> PFU of NiV (5 or 6 animals per group). (A) Survival of mice infected by NiV was followed up for 24 days. \*P < 0.05 (MyD88/TRIF/MAVS/STING KO vs WT), †P < 0.05 (IFNAR KO vs WT) and ‡P < 0.01 (MyD88/TRIF/MAVS KO vs MyD88/TRIF/MAVS/STING KO) (Gehan-Breslow-Wilcoxon test). (B) Immunohistochemistry of murine brains following NiV infection. Brains of WT mouse, IFNAR KO mouse, MyD88/TRIF/MAVS KO and MyD88/TRIF/MAVS/STING KO were collected on days 2, 6, 13 and 11 respectively. Scale bars represent 100 μm. (C-E) Expression of NiV nucleoprotein (NiV-N) in the brain of NiV-infected mice, harvested on the day of death or euthanized at the end of protocol for different genotypes, was determined by RT-qPCR. Results represent mean and standard errors for each group. Analysis of IFNβ and IFNα expression by RT-qPCR in organs harvested 2–13 days after infection. All samples were analyzed using One-way analysis of variance, followed by the Tukey multiple comparisons test, \*P < 0.05 compared to WT condition.

### STING controls NiV replication in primary murine embryonic fibroblasts (pMEFs).

To further evaluate the role of STING during NiV infection in mice, we analyzed the impact of the gene deletion of various nodal adaptors on the *in vitro* NiV replication in pMEFs. The pMEFs were generated from mice bearing the corresponding deleted genes as described previously (Brune et al., 2001). They were infected with rNiV-eGFP to allow imaging of the viral infection by fluorescent microscopy. In agreement with the above *in vivo* observations, MyD88 KO and MyD88/TRIF KO pMEFs were able to control NiV replication as well as WT pMEFs, with only few observed infected cells. In contrast, NiV rapidly spreads within the culture of MyD88/TRIF/MAVS KO and MyD88/TRIF/MAVS/STING KO pMEFs although not as extensively as in IFNAR KO cells (Figure 2A). Moreover, single STING KO pMEFs were also unable to control the viral spread, highlighting a major role of STING in the mouse innate defense against NiV infection (Figure 2A). The poor permissiveness of WT, MyD88 KO and MyD88/TRIF KO cells was confirmed by a low amount of viral RNA in these cells (Figure 2B) and limited release of viral RNA in the supernatant (Figure 2C). These three cell types exhibited comparable amounts of IFNβ mRNA (Figure 2D) while this mRNA was nearly undetectable in non-infected WT cells. However, contrary to WT pMEFs which exhibit a significant increase in IFNα, the infection of MyD88 KO and MyD88/TRIF KO cells did not result in a significant accumulation of IFNα mRNA (Figure 2E). The infection of IFNAR KO cells was associated

159 with elevated cytoplasmic and released viral RNA as well as elevated levels of both IFN $\beta$  and IFN $\alpha$   
 160 mRNA as expected since all four induction axes of innate immunity are functional but unable to  
 161 activate an efficient antiviral program (**Figure 2B-E**). In contrast, no accumulation of either IFN $\beta$  or  
 162 IFN $\alpha$  occurred concurrently to the high levels of NiV-N RNA (**Figure 2B-C**) observed in infected  
 163 MyD88/TRIF/MAVS KO and MyD88/TRIF/MAVS/STING KO (**Figure 2D-E**). In STING KO pMEFs,  
 164 despite lower levels than IFNAR KO cells, high amounts of NiV-N RNA accumulated in the cytoplasm  
 165 compared to WT cells (**Figure 2B**). This intermediate phenotype of STING KO cells was associated  
 166 with no significant IFN $\beta$  mRNA induction, but high levels of IFN $\alpha$  mRNA (**Figure 2D-E**). Altogether,  
 167 these results indicate that in murine pMEFs (i) the control of NiV infection is mediated by IFN-I-  
 168 mediated activation of an antiviral program, (ii) the IFN $\beta$  and IFN $\alpha$  response plays a major and minor  
 169 role, respectively, in this process, (iii) STING is necessary for the induction of IFN $\beta$ , but not of IFN $\alpha$ ,  
 170 and (iv) MAVS, in combination with MyD88 or not, is important for the activation of IFN-I genes  
 171 confirming our previous observations (Iampietro et al., 2020).

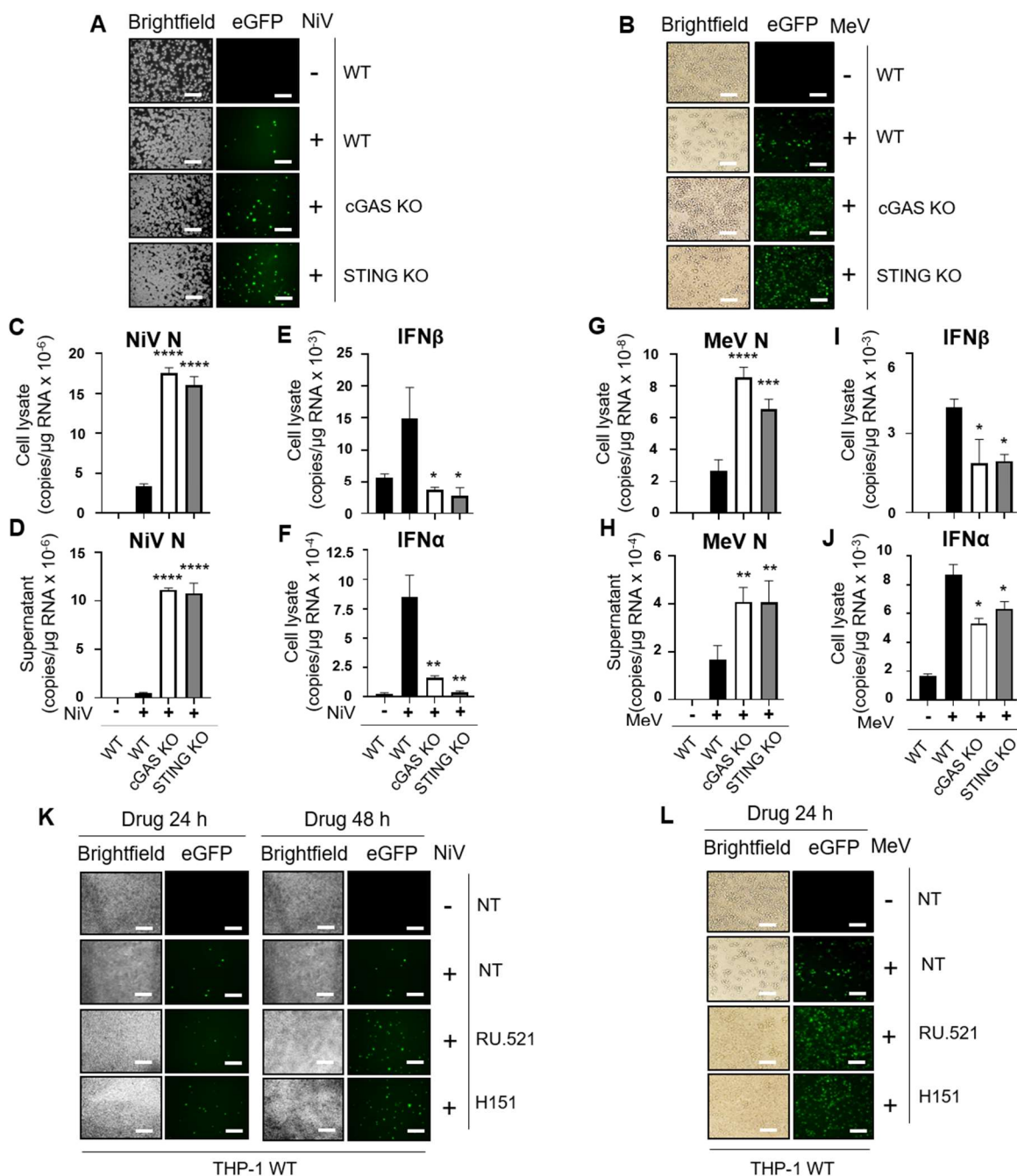


172  
 173 **Figure 2. STING controls NiV replication in primary murine embryonic fibroblasts (pMEFs).** pMEFs obtained from mice deficient in  
 174 the indicated signaling pathways were infected with rNiV-eGFP (MOI of 0.3) and cultured for 24 h. (A) Cells were analyzed for eGFP  
 175 expression by fluorescence microscopy. Scale bars represent 100  $\mu$ m. (B-E) Cells and supernatants were harvested and analyzed by  
 176 RT-qPCR for NiV-N (B and C), IFN $\beta$  (D), and IFN $\alpha$  (E) expression. Results are presented as means  $\pm$  standard errors. The statistical  
 177 significance of differences between infected wild-type (WT) cells and knockout (KO) cells was analyzed using 1-way analysis of  
 178 variance, followed by the Tukey multiple comparisons test. \* $P < 0.05$ ; \*\* $P < 0.01$ ; \*\*\* $P < 0.001$ ; \*\*\*\* $P < 0.0001$  compared to NiV-  
 179 infected WT condition.

180  
 181 **cGAS/STING pathway has a critical role in the control of paramyxovirus infection in human THP-1**  
 182 **cells.**

183 The role of STING and its upstream activator cGAS in the innate response to NiV was further  
 184 explored in the human monocytic THP-1 cell line that was either WT or deficient in cGAS (cGAS KO)  
 185 or STING (STING KO). WT THP-1 cells have the advantage to exhibit a limited permissiveness to  
 186 infection with both NiV and the WT derived recombinant MeV strain rMeV-EdmH-eGFP another  
 187 member of the *Paramyxoviridae* family belonging to the closely related *morbillivirus* genus. This  
 188 virus expresses the Edmonston vaccine-derived H glycoprotein allowing the use of ubiquitously

189 expressed CD46 as cellular receptor (Naniche et al., 1993) and hence enters into THP-1 cells that do  
 190 not or minimally express the known physiological MeV receptors CD150 and Nectin 4 (Crimeen-  
 191 Irwin et al., 2003; Noyce et al., 2011; Tatsuo et al., 2000). THP-1 cells depleted of cGAS or STING  
 192 exhibited enhanced permissiveness to NiV and MeV infections when compared to their WT  
 193 counterparts (**Figure 3A, 3B, S2A and S2B**). This was analyzed by fluorescence imaging of NiV  
 194 propagation throughout the cell culture (**Figure 3A**), by the proportions of THP-1 infected cells as  
 195 determined by flow cytometry (**Figure S2A**), and by the quantification of viral N RNA by RT-qPCR  
 196 both in cell extracts (**Figure 3C**) and released in the cell supernatants (**Figure 3D**). Correlatively, and  
 197 in agreement with observations made in pMEFs infected with NiV, the higher permissiveness of  
 198 cGAS KO and STING KO THP-1 cells was associated with the abolition of IFN $\beta$  and/or IFN $\alpha$  mRNA  
 199 accumulation (**Figure 3E-F**). Comparable results were obtained after infection by MeV although a  
 200 reduced but significant accumulation of both IFN $\beta$  and IFN $\alpha$  mRNA was still observed in cGAS KO  
 201 and STING KO cells (**Figure 3G-J**).  
 202



203

204 **Figure 3. cGAS/STING pathway has a critical role in the control of paramyxovirus infection in human THP-1 cells.** THP-1 cells  
205 deficient in the indicated signaling pathways were infected with NiV-eGFP and MeV-eGFP (MOI of 0.1) for 48 h and 24 h respectively.  
206 (A-B) Cells were analyzed for eGFP expression by fluorescence microscopy. (C-J) Cell lysates and/or supernatants were harvested and  
207 analyzed by RT-qPCR for the expression of NiV-N (C and D), MeV-N (G and H), IFN $\beta$  (E and I), and IFN $\alpha$  (F and J). Results are presented  
208 as means  $\pm$  standard errors. THP-1 WT cells treated or not (NT) with the specific inhibitors for cGAS (RU.521) or STING (H151) were  
209 infected with NiV-eGFP and MeV-eGFP (MOI of 0.1) for 24 h and 48 h. (K and L) Cells were analyzed for eGFP expression by  
210 fluorescence microscopy. Scale bars represent 100  $\mu$ m. The statistical significance of differences between infected WT and KO cells  
211 was analyzed using 1-way analysis of variance, followed by the Tukey multiple comparisons test. \* $P$  < 0.05; \*\* $P$  < 0.01; \*\*\* $P$  < 0.001;  
212 \*\*\*\* $P$  < 0.0001 compared to infected WT condition.

213  
214 As an alternative and complementary approach, we analyzed the paramyxoviral propagation  
215 within WT THP-1 cells treated with selective inhibitors of cGAS and STING, namely RU-521 and H151  
216 drugs, respectively. RU.521 is a competitive inhibitor of ATP and GTP substrates for binding to the  
217 cGAS catalytic pocket that prevents their cyclisation into cGAMP (Vincent et al., 2017; Xie et al.,  
218 2019). H151 covalently binds to STING Cys91, inhibits the palmitoylation of STING and consequently  
219 the activation of IFN-I production (Haag et al., 2018). Addition of RU-521 or H151 one hour prior to  
220 the infection resulted in an improved propagation of NiV and MeV as evidenced by fluorescence  
221 microscopy (**Figure 3K and 3L**) and flow cytometry (**Figure S2C, S2D, S2E**).

222 Thus, the cGAS/STING axis also appears to play a critical role in human cells to control  
223 paramyxovirus infections by allowing the expression of IFN $\beta$  and to a lower extent that of IFN $\alpha$ .

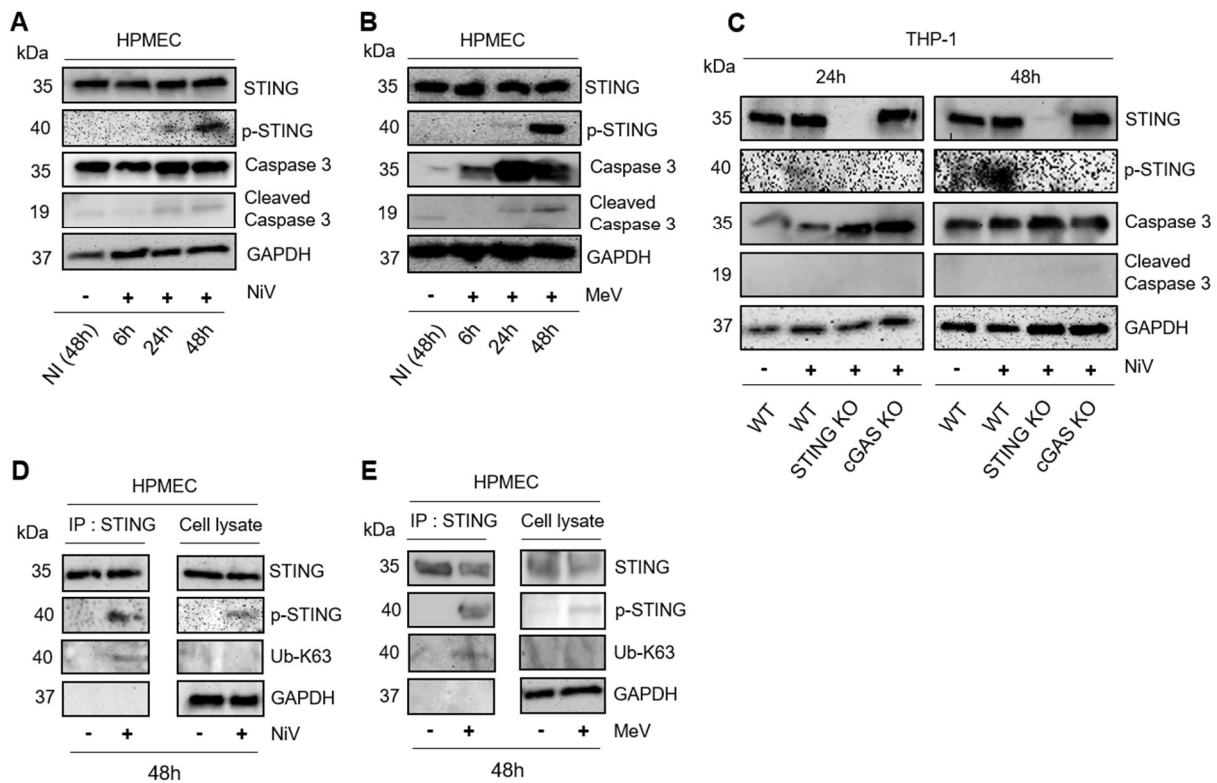
### 224 **Paramyxovirus infection activates the cGAS/STING pathway in both murine and human cells.**

225 The increased viral infection observed upon abolition of either cGAS or STING suggested that  
226 paramyxoviruses could activate STING. This was investigated by analyzing specific phosphorylation  
227 and/or ubiquitination of activated STING in pMEFs, THP-1 and human pulmonary microvascular  
228 endothelial cells (HPMEC) as representative of primary targets of NiV infection in humans (**Figure 4**  
229 **and S3**). A time course follow up of the activation of cGAS/STING axis induced by viral infection was  
230 performed at 6, 24 and 48 hours post-infection (h.p.i.) by western blot using antibodies against  
231 STING-S366<sup>P</sup> (Chiang and Gack, 2017). While the expression level of STING remained unchanged  
232 throughout the 48h observation, moderate amounts of STING-S366<sup>P</sup> became detectable at 24 h.p.i.  
233 and further increased at 48 h.p.i. after NiV or MeV infection of HPMECs (**Figure 4A and 4B**) and THP-  
234 1 cells (**Figure 4C and S3A**). Importantly, STING-S366<sup>P</sup> was not detected in NiV- or MeV-infected  
235 cGAS KO THP-1 cells at 24 and 48 h.p.i., and as expected in STING KO THP-1 cells (**Figure 4C and**  
236 **S3A**). Accordingly, STING-S366<sup>P</sup> was also not detected in THP-1 cells infected and treated with either  
237 RU-521 or H151 (**Figure S3A**).

238 Accordingly, while uninfected WT pMEFs, NiV-infected STING KO and  
239 MyD88/TRIF/MAVS/STING KO cells did not elicit any mouse STING-S365<sup>P</sup> band (Tsuchiya et al.,  
240 2016), NiV-infected WT and MyD88/TRIF/MAVS KO pMEFs displayed activation of STING protein  
241 (**Figure S3B**). Importantly, the detection of the STING-S365<sup>P</sup> band in MyD88/TRIF/MAVS KO pMEFs  
242 indicates that NiV infection activates the STING signaling pathway independently from the TLR-  
243 MyD88/TRIF and RLR/MAVS pathways of innate immunity. Since K63-linked ubiquitination (Ub-K63)  
244 is another hallmark of STING activation, mainly associated to the activation of NF- $\kappa$ B (Chiang and  
245 Gack, 2017), STING ubiquitination was also evaluated in HPMECs infected for 48 h with NiV or MeV.  
246 STING immunoprecipitated using anti-STING antibodies was found to be labelled by both anti-STING-  
247 S366<sup>P</sup> and anti-Ub-K63 antibodies (**Figure 4D and 4E**). As an apoptotic environment could activate  
248 STING in bystander cells (Ahn et al., 2012), a potential effect of viral-induced cell death in infected  
249 cultures was evaluated by analyzing caspase 3 activity. The levels of cleaved caspase 3 were  
250 minimally increased between uninfected and NiV- or MeV-infected cells, indicating that cell death  
251 had likely a minor impact on STING activation until 48 h post-infection (**Figure 4A, 4B, S3A, S3B, S3C**  
252 **and S3D**).

254  
255  
256

We conclude that negative strand RNA paramyxoviruses activate the cGAS/STING axis to trigger the innate immune responses.



257

258

259

260

261

262

263

264

265

266

267

268

269

270

271

272

273

274

275

276

277

278

279

280

281

282

283

**Figure 4. Paramyxovirus infection activates the cGAS/STING pathway in human cells.** Human pulmonary microvascular endothelial (HPMEC) cells and THP-1 cells deficient in the indicated signaling platforms were infected with either NiV or MeV (MOI of 1) for 6, 24 or 48 h. (A-C) Cells were analyzed for phospho-STING (p-STING), STING, Caspase 3, cleaved Caspase 3 and GAPDH expression by western blot analysis. (D-E) HPMEC cells were infected with NiV (D) and MeV (E) (MOI of 1) for 48 h before cell lysis. Endogenous STING was immunoprecipitated using anti-STING antibodies followed by western blot analyses using anti-STING, anti-Ub-K63, anti p-STING and anti-GAPDH antibodies. In parallel, endogenous expression levels of STING, p-STING and Ub-K63 together as GAPDH as loading control in cell lysates were analyzed by western blot. Shown data are representative of three independent experiments showing similar results.

## DISCUSSION

Although its role in response to DNA virus infection has been well deciphered (Eaglesham and Kranzusch, 2020), the role of cGAS/STING against RNA viruses such as paramyxoviruses is poorly understood. While cGAS was reported to interact with dsRNA, no production of cGAMP was detected, thus cGAS could not canonically activate STING directly (Civril et al., 2013). However, previous studies have shown interactions between RNA viruses and cGAS/STING in (i) their control by innate immunity or (ii) their capacity to disrupt the cGAS/STING pathway, reflecting a likely role of STING in the host response (Aguirre et al., 2017; Franz et al., 2018; Ishikawa et al., 2009; Schoggins et al., 2014).

As paramyxoviruses replicate within the cytoplasm using their own RNA-dependent RNA polymerase, i.e. their replicative cycle does not rely on a DNA intermediate step (Gerlier and Lyles, 2011). Because cGAS is exclusively activated upon binding to dsDNA (Kranzusch et al., 2013; Sun et al., 2013) or DNA/RNA hybrid (Mankan et al., 2014), we have to speculate about the identity of the cGAS agonist during infection by paramyxoviruses. The possibility of mitochondrial release of DNA at some stage of the viral infection as evidenced after infection with Dengue virus, a positive stranded RNA virus (Aguirre et al., 2017; Sun et al., 2017), will have to be explored.



284 Collectively, the obtained data fit with a model where the infection by NiV or MeV activates,  
285 the cGAS/STING pathway. This activation results in the induction of the IFN $\beta$  and possibly the IFN $\alpha$   
286 gene (see below) that mediate the activation of an efficient antiviral program in *in vitro* and *in vivo*  
287 mouse models and/or in human cells closely mimicking what happens after the infection by mouse  
288 cytomegalovirus (MCMV), a DNA virus (Tegtmeyer et al., 2019). Notably, the comparison of the  
289 phenotype of triple and quadruple KO pMEFs indicate that the cGAS/STING pathway strongly  
290 reinforces (or even conditions) the activation of type I IFN responses via the TLR8/MyD88 and/or  
291 the RLR/MAVS pathway by paramyxoviruses, including MeV (Ikegame et al., 2010; Runge et al.,  
292 2014; Seth et al., 2005).

293 STING can bind to RIG-I and MAVS (Sun et al., 2012) and is thought to potentiate the  
294 RLR/MAVS signaling leading to the activation of type I IFN (Ishikawa et al., 2009; Zevini et al., 2017;  
295 Zhong et al., 2008). The present data fits with this model. The defect of the cGAS/STING pathway  
296 strongly facilitates the replication of NiV and MeV as expected from the observed loss in activating  
297 the IFN-I response. We cannot exclude that this facilitation results also from the concomitant  
298 disappearance of a STING-dependent inhibition of the translation of viral protein as recently  
299 reported (Franz et al., 2018). However, they reported that the absence of STING modestly affects  
300 the IFN response to the infection by negative stranded RNA viruses compared to the present work.

301 Upon infection of MeV and/or NiV in mouse and/or human cells, the absence of the  
302 cGAS/STING pathway affect the IFN $\beta$  response and to a lower and more variable extend the IFN $\alpha$   
303 response. Due to cell-dependent ability to produce IFN $\alpha$ , different outcome may reflect higher  
304 expression of IRF-7 in pMEFs (Sharma et al., 2019) compared to THP-1 cells (Green et al., 2020).  
305 Indeed, while the activation of the IFN $\beta$  gene optimally relies on IRF3 homodimers or IRF3/IRF7  
306 heterodimers and NF- $\kappa$ B (Honda et al., 2005; Wathélet et al., 1998) that of the IFN $\alpha$  genes relies  
307 mostly on IRF7 homodimers (Yeow et al., 2000). Interestingly, STING mostly targets IRF-3 (Zhong et  
308 al., 2008) and NF- $\kappa$ B (Stempel et al., 2019) and consequently STING preferentially activates IFN $\beta$ .

309 Our study demonstrates that STING is activated against RNA viruses as also recently reported  
310 with SARS-CoV-2 (Neufeldt et al., 2020) and highlights that STING is modified and activated through  
311 S366 phosphorylation and/or K-63 linked ubiquitination during NiV and MeV infection. Additional  
312 studies will uncover the occurrence of others PMTs modification, STING subcellular location and the  
313 source of the cognate DNA that activate cGAS during RNA virus infection.

314 In conclusion, cGAS/STING activation occurs during paramyxovirus infections, both *in vitro*  
315 and *in vivo*. This highlights an undefined aspect of the immune regulation against negative strand  
316 viruses and reveals cGAS/STING as potential targets in the development of novel antiviral strategies.

317

## 318 **METHODS**

319

### 320 **Mice**

321 Several lines of transgenic mice, all in C57BL/6 genetic background, were used: wild type (WT)  
322 C57BL/6J mice and following knockout (KO) models: mice deleted for IFN-I receptor (IFNAR-KO)  
323 (Muller et al., 1994), TLR adaptor protein MyD88 (MyD88-KO) (Adachi et al., 1998), and mice  
324 crossed to bear several deletions, including MyD88/TRIF-KO (Waibler et al., 2007),  
325 MyD88/TRIF/MAVS-KO (Spanier et al., 2014) and MyD88/TRIF/MAVS/STING KO (Tegtmeyer et al.,  
326 2019).

327

### 328 **Infection of mice**

329 Groups of 5–10 mice from each line, 4–6 weeks of age, were anesthetized with isoflurane and  
330 infected intraperitoneally with  $10^6$  PFUs of Nipah virus Malaysia strain, contained in a 200  $\mu$ L  
331 volume. Animals were monitored for 24 days after infection and manipulated in accordance to

332 good experimental practice and approved by the regional ethics committee CECCAPP (Comité  
333 d'Evaluation Commun au Centre Léon Bérard, à l'Animalerie de transit de l'ENS, au PBES et au  
334 laboratoire P4) and authorized by the French Ministry of Higher Education and Research (no.  
335 00962.01). Animal experiments were conducted by the animal facility team in the INSERM Jean  
336 Mérieux BSL-4 laboratory in Lyon, France.

337

### 338 **Cell Lines**

339 Primary murine embryonic fibroblasts (pMEFs) were isolated from murine embryos obtained from  
340 pregnant mice 13 days after conception, as described elsewhere (Brune et al., 2001) and cultured in  
341 Dulbecco's modified Eagle's medium (DMEM) GlutaMAX supplemented with 10% heat-inactivated  
342 fetal bovine serum (FBS), 0.2% 2-mercaptoethanol, 1% HEPES, 1% nonessential amino acids, 1%  
343 sodium pyruvate, and 2% penicillin-streptomycin mix. For infections, pMEFs were plated in 12-well  
344 plates at  $2 \cdot 10^5$  cells per well and cultured with rNiV-eGFP at a multiplicity of infection (MOI) of 0.3  
345 plaque-forming units (PFUs)/cell for 1 h at 37°C. Virus-containing medium was then removed, and  
346 cells were washed once with 1× phosphate-buffered saline. Finally, fresh DMEM was added to cells  
347 that were incubated for 24 h at 37°C. Human monocytic THP-1 cell lines were obtained as described  
348 previously and cultured in RPMI 1640 GlutaMAX supplemented with 10% heat-inactivated FBS, 1%  
349 HEPES and 2% of penicillin-streptomycin mix. Human pulmonary microvascular endothelial cells  
350 (HPMEC) (Krump-Konvalinkova et al., 2001) were cultured in Endothelial Cell Growth Medium, in  
351 flasks coated with 0,1% bovine gelatine in PBS. For infection, HPMECs were plated in 12-well plates  
352 at  $2 \cdot 10^5$  cells per well and cultured with rNiV-eGFP or rMeV-edmH-eGFP at a MOI of 1 PFUs/cell for  
353 24 or 48 hours at 37°C. All cell types were incubated at 37°C with 5% CO<sub>2</sub> and were tested negative  
354 for Mycoplasma spp.

### 355 **Drugs**

356 H151, a specific inhibitor for STING and RU.521, a specific inhibitor for cGAS were added 1 h previous  
357 infection of THP-1 cells at 10 μM and 10 μg/ml, respectively, selected according to the previously  
358 published results (Chang et al., 2020; Hayden et al., 2020). Then, cells were infected with rNiV-eGFP  
359 or rMeV-edmH-eGFP and incubated for 24 or 48 h at 37°C with 5% CO<sub>2</sub>.

### 360 **Viruses**

361 NiV Malaysia (isolate UMMC1; GeneBak AY029767, recombinant NiV (rNiV)-enhanced green  
362 fluorescent protein (eGFP) (Yoneda et al., 2006) and recombinant MV IC323 vaccine strain,  
363 expressing Edmonston H and eGFP (Hashimoto et al., 2002), kindly provided by Dr Y. Yanagi (Kyushu  
364 University, Japan) and were prepared by infecting Vero-E6 cells, in the INSERM Jean Mérieux  
365 biosafety level 4 (BSL-4) and BSL-2 laboratories at CIRI in Lyon, France respectively.

### 366 **Immunohistochemistry**

367 Brains from mice were embedded in paraffin wax and sectioned at 7 μm. Slides were deparaffinated  
368 and rehydrated in three Xylene baths for 5 min each, followed by two 100% alcohol baths for 5 min,  
369 and then succeeded with multiple baths using decreasing level of alcohol for 3 min each. After  
370 deparaffination, slides were put in a sodium citrate solution in a boiling water bath for 20 min for  
371 heat-induced epitope retrieval and washed 3 times in PBS for 3 min afterwards. Activity of  
372 endogenous peroxidase was blocked using a H<sub>2</sub>O<sub>2</sub> 0.3% solution. Blocking of non-specific epitopes

373 is done using PBS-2.5% decomplexed Normal Horse Serum + 0.15% Triton X-100 for 30 min.  
374 Then, primary rabbit anti-NiV N antibody was used at 1/10000 dilution and incubated overnight at  
375 4°C in the blocking buffer. For secondary antibody and revealing steps, ImmPress system (anti-rabbit  
376 ig/peroxydase) was used. Counterstaining was performed using Harris solution and photographs  
377 were taken with a microscope Zeiss Axiovert 100M.

378

### 379 **Co-immunoprecipitations**

380 HPMEC cells ( $5 \times 10^5$ ) were seeded in 6-well plates. 16 h after seeding, cells were infected with the  
381 appropriate dilution of rNiV-eGFP or rMeV-edmH-eGFP at a MOI of 1 in RPMI described above.  
382 Forty-eight hours post-infection, cells were lysed in RIPA buffer, supplemented with a cocktail of  
383 protease-phosphatase inhibitors for 30 min on ice, and centrifuged for 10 min at 4°C at 15,000 g.  
384 Supernatants were incubated with a rabbit anti-STING antibody for 2 h at 4°C. Then, protein A/G  
385 agarose beads were added to the mix overnight at 4°C. Beads were then washed three times in  
386 washing buffer (RIPA buffer, supplemented with a cocktail of protease-phosphatase inhibitor), and  
387 proteins were eluted in 100 µl of elution buffer (Reducing agent 10X, Laemmli 4X, RIPA buffer,  
388 supplemented with a cocktail of protease-phosphatase inhibitors) for 15 min at 96°C. Then the  
389 eluate and a sample of input of the cell extract were run on polyacrylamide gel electrophoresis (SDS-  
390 PAGE) and analyzed by western-blotting.

391

### 392 **Immunoblot Analysis**

393 Heated protein lysates were separated by 4-15% SDS-PAGE and electro transferred for 1 h onto  
394 polyvinylidene difluoride (PVDF) membranes at 4°C. PVDF membranes were blocked in Tris-buffered  
395 saline containing 0.05% Tween 20 (TBS-T) + 5% milk for 1 h and then incubated overnight with  
396 primary antibodies, mouse anti-GAPDH, rabbit anti-STING, rabbit anti-human S366 p-STING, rabbit  
397 anti-mouse S365 p-STING, rabbit anti-Caspase 3, rabbit anti-cleaved Caspase 3 and rabbit anti-Ub-  
398 K63 antibodies, diluted 1:1000 in TBS-T + 0.2% milk. Membranes were then washed 3 times using  
399 TBS-T and incubated on an additional 1 h with horseradish peroxydase conjugated anti-mouse or  
400 anti-rabbit IgG antibodies (diluted 1:5000 in TBS-T + 5% milk). Membranes were then washed 5  
401 times in TBS-T, incubated in Super Signal West Dura to stain cell lysates or in Super Signal West  
402 Femto reagent to stain bead eluates. Chemiluminescent signals were measured with the VersaDoc  
403 and ChemiDoc Imaging System.

404

### 405 **RNA Extraction and RT-qPCR**

406 At indicated time points, cells and supernatants were collected and RNA extracted using appropriate  
407 NucleoSpin RNA Kits according to the manufacturer's instructions and yield and purity of extracted  
408 RNA was assessed using the DS-11-FX spectrophotometer. Equal amounts of extracted RNA (500 ng)  
409 were reverse transcribed using the iScript Select cDNA Synthesis Kit and amplified by real-time PCR  
410 using Platinum SYBR Green qPCR SuperMix-UDG on a StepOnePlus Real-Time PCR System. Data  
411 were analyzed using StepOne software and calculations were done using the  $2^{-\Delta\Delta CT}$  method.  
412 Expression was normalized to that of glyceraldehyde 3-phosphate dehydrogenase (GAPDH) and  
413 expressed as copies of mRNA. Specific set of primers were designed and validated for the detection

414 of human hGAPDH, hIFN $\alpha$  and hIFN $\beta$ , murine mGAPDH, murine mIFN $\alpha$  and mIFN $\beta$  and viral NiV N  
415 and MeV N.

416

#### 417 **Immunofluorescence**

418 For PMEFs and THP-1 infections,  $3 \times 10^5$  and  $5 \times 10^5$  cells were seeded in 12-well plates, respectively,  
419 before being infected with rNiV-eGFP and rMeV-edmH-eGFP at a MOI of 0.3 or 0.1 and cultured for  
420 24 or 48 h at 37°C with 5% CO<sub>2</sub>. Then, cells were evaluated for eGFP expression using a Zeiss  
421 Axiovert 100M microscope in the BSL-4 or a NIKON Eclipse Ts2R in the BSL-2, and photographs were  
422 taken 24 and 48 h after infection and treated using ImageJ software version Java 1.8.0\_112.

423

#### 424 **Flow cytometry**

425 THP-1 cells were seeded in 12-well plates at  $3 \times 10^5$  and  $5 \times 10^5$  per well before being infected with  
426 rNiV-eGFP and rMeV-edmH-eGFP at a MOI of 0.1 and cultured for 24 or 48 h at 37°C with 5% CO<sub>2</sub>.  
427 Then, cells were washed, reconstituted in PBS 1X and evaluated for eGFP expression using a Gallios  
428 flow cytometer in the BSL-4 or a 4L Fortessa flow cytometer. Analyses were performed 24 and 48 h  
429 after infection.

430

#### 431 **Ethical statement**

432 Animals were handled in strict accordance with good animal practice as defined by the French  
433 national charter on the ethics of animal experimentation and all efforts were made to minimize  
434 suffering. Animal work was approved by the Regional ethical committee and French Ministry of High  
435 Education and Research and experiments were performed in the INSERM Jean Mérieux BSL-4  
436 laboratory in Lyon, France (French Animal regulation committee N° 00962.01).

437

#### 438 **Analysis of eGFP quantification in THP-1 cells**

439 The results are presented in the form of histograms which represent the mean eGFP positive cells  
440 for each conditions and error bars represent the standard errors (SE) for n=3 experimental  
441 replicates. The different conditions were compared to the control (WT+). Statistical significance was  
442 assessed by a one-way ANOVA, followed by a Tukey's multiple comparisons test; \*p < 0.05, \*\*p <  
443 0.01, \*\*\*p < 0.001 and \*\*\*\*p < 0.0001 (threshold of significance of 5%).

444

#### 445 **qPCR analysis**

446 The results are presented in the form of histograms, which represent the mean of copies of mRNA  
447 for a gene for each condition and error bars represent the standard errors (SE) for n=3 experimental  
448 replicates. The different conditions were compared to the control (WT+). Statistical significance was  
449 assessed by a one-way ANOVA, followed by a Tukey's multiple comparisons test; \*p < 0.05, \*\*p <  
450 0.01, \*\*\*p < 0.001 and \*\*\*\*p < 0.0001 (threshold of significance of 5%).

451

#### 452 **Densitometry**

453 Densitometric analysis of cleaved caspase 3 immunoblots from three independent experiments  
454 were performed using the VersaDoc Imaging System (Bio-Rad) and analyzed with ImageJ 1.52p Fiji  
455 package software (<https://imagej.net/Fiji>). GAPDH expression was used for normalization.

456

457 **ACKNOWLEDGEMENTS**

458 The work was supported by INSERM, LABEX ECOFECT (ANR-11-LABX-0048) of Lyon University, within  
459 the program "Investissements d'Avenir" (ANR-11-IDEX-0007) operated by the French National  
460 Research Agency (ANR), by ANR-18-CE11-0014-02, by Aviesan Sino-French agreement on Nipah  
461 virus study. We thank the entire animal experimentation team of INSERM "Jean Mérieux" BSL4  
462 laboratory for the realization of the animal experiment and the biosafety team for their assistance  
463 for BSL4 activities. We are grateful to all the members of the group Immunobiology of viral infection  
464 at CIRI, for the help in the realization of this study. We acknowledge the contribution of the SFR  
465 Biosciences (UMS3444/CNRS, US8/INSERM, ENS de Lyon, UCBL) flow cytometry facility.

466

467 **AUTHOR CONTRIBUTIONS**

468 MI, UK and BH designed the study. MI, CD, CM, JR, AC, SD, KD, NA and SM performed experiments.  
469 MI, CM, JS, DG and BH analyzed the data. MI, JS, DG and BH wrote the article. MI, JS, DG and BH  
470 prepared the figures. MF, RP, JS and UK provided some essential tools.

471

472 **DECLARATION OF INTERESTS**

473 The authors declare no competing interests.

474

475 **REFERENCES**

476 Aguirre, S., Luthra, P., Sanchez-Aparicio, M.T., Maestre, A.M., Patel, J., Lamothe, F., Fredericks,  
477 A.C., Tripathi, S., Zhu, T., Pintado-Silva, J., et al. (2017). Dengue virus NS2B protein targets cGAS  
478 for degradation and prevents mitochondrial DNA sensing during infection. *Nat Microbiol* 2, 17037.

479 Ahn, J., Gutman, D., Saijo, S., and Barber, G.N. (2012). STING manifests self DNA-dependent  
480 inflammatory disease. *Proceedings of the National Academy of Sciences* 109, 19386–19391.

481 Akira, S., Uematsu, S., and Takeuchi, O. (2006). Pathogen recognition and innate immunity. *Cell*  
482 124, 783–801.

483 Baccala, R., Gonzalez-Quintal, R., Lawson, B.R., Stern, M.E., Kono, D.H., Beutler, B., and  
484 Theofilopoulos, A.N. (2009). Sensors of the innate immune system: their mode of action. *Nat Rev*  
485 *Rheumatol* 5, 448–456.

486 Borden, E.C., Sen, G.C., Uze, G., Silverman, R.H., Ransohoff, R.M., Foster, G.R., and Stark, G.R.  
487 (2007). Interferons at age 50: past, current and future impact on biomedicine. *Nat Rev Drug Discov*  
488 6, 975–990.

489 Brune, W., Hengel, H., and Koszinowski, U.H. (2001). A mouse model for cytomegalovirus  
490 infection. *Curr Protoc Immunol Chapter 19*, Unit 19.7.

491 Chiang, C., and Gack, M.U. (2017). Post-translational Control of Intracellular Pathogen Sensing  
492 Pathways. *Trends Immunol* 38, 39–52.

493 Civril, F., Deimling, T., de Oliveira Mann, C.C., Ablasser, A., Moldt, M., Witte, G., Hornung, V.,  
494 and Hopfner, K.-P. (2013). Structural mechanism of cytosolic DNA sensing by cGAS. *Nature* 498,  
495 332–337.

496 Cong, X., Yuan, Z., Du, Y., Wu, B., Lu, D., Wu, X., Zhang, Y., Li, F., Wei, B., Li, J., et al. (2019).  
497 Crystal structures of porcine STING<sup>CBD</sup>-CDN complexes reveal the mechanism of ligand  
498 recognition and discrimination of STING proteins. *J. Biol. Chem.* 294, 11420–11432.

- 499 Crimeen-Irwin, B., Ellis, S., Christiansen, D., Ludford-Menting, M.J., Milland, J., Lanteri, M.,  
500 Loveland, B.E., Gerlier, D., and Russell, S.M. (2003). Ligand binding determines whether CD46 is  
501 internalized by clathrin-coated pits or macropinocytosis. *J. Biol. Chem.* *278*, 46927–46937.
- 502 Der, S.D., Zhou, A., Williams, B.R., and Silverman, R.H. (1998). Identification of genes  
503 differentially regulated by interferon alpha, beta, or gamma using oligonucleotide arrays. *Proc Natl*  
504 *Acad Sci U S A* *95*, 15623–15628.
- 505 Dhondt, K.P., Mathieu, C., Chalons, M., Reynaud, J.M., Vallve, A., Raoul, H., and Horvat, B.  
506 (2013). Type I interferon signaling protects mice from lethal henipavirus infection. *J. Infect. Dis.*  
507 *207*, 142–151.
- 508 Dobbs, N., Burnaevskiy, N., Chen, D., Gonugunta, V.K., Alto, N.M., and Yan, N. (2015). STING  
509 Activation by Translocation from the ER Is Associated with Infection and Autoinflammatory  
510 Disease. *Cell Host & Microbe* *18*, 157–168.
- 511 Eaglesham, J.B., and Kranzusch, P.J. (2020). Conserved strategies for pathogen evasion of cGAS-  
512 STING immunity. *Curr Opin Immunol* *66*, 27–34.
- 513 Ergun, S.L., Fernandez, D., Weiss, T.M., and Li, L. (2019). STING Polymer Structure Reveals  
514 Mechanisms for Activation, Hyperactivation, and Inhibition. *Cell* *178*, 290-301.e10.
- 515 Ferren, M., Horvat, B., and Mathieu, C. (2019). Measles Encephalitis: Towards New Therapeutics.  
516 *Viruses* *11*.
- 517 Franz, K.M., Neidermyer, W.J., Tan, Y.-J., Whelan, S.P.J., and Kagan, J.C. (2018). STING-  
518 dependent translation inhibition restricts RNA virus replication. *Proc Natl Acad Sci USA* *115*,  
519 E2058–E2067.
- 520 Gao, P., Ascano, M., Wu, Y., Barchet, W., Gaffney, B.L., Zillinger, T., Serganov, A.A., Liu, Y.,  
521 Jones, R.A., Hartmann, G., et al. (2013). Cyclic [G(2',5')pA(3',5')p] Is the Metazoan Second  
522 Messenger Produced by DNA-Activated Cyclic GMP-AMP Synthase. *Cell* *153*, 1094–1107.
- 523 Gerlier, D., and Lyles, D.S. (2011). Interplay between innate immunity and negative-strand RNA  
524 viruses: towards a rational model. *Microbiol Mol Biol Rev* *75*, 468–490, second page of table of  
525 contents.
- 526 Green, I.D., Pinello, N., Song, R., Lee, Q., Halstead, J.M., Kwok, C.-T., Wong, A.C.H., Nair, S.S.,  
527 Clark, S.J., Roediger, B., et al. (2020). Macrophage development and activation involve coordinated  
528 intron retention in key inflammatory regulators. *Nucleic Acids Research* *48*, 6513–6529.
- 529 Gui, X., Yang, H., Li, T., Tan, X., Shi, P., Li, M., Du, F., and Chen, Z.J. (2019). Autophagy  
530 induction via STING trafficking is a primordial function of the cGAS pathway. *Nature* *567*, 262–  
531 266.
- 532 Haag, S.M., Gulen, M.F., Reymond, L., Gibelin, A., Abrami, L., Decout, A., Heymann, M., van der  
533 Goot, F.G., Turcatti, G., Behrendt, R., et al. (2018). Targeting STING with covalent small-molecule  
534 inhibitors. *Nature* *559*, 269–273.
- 535 Honda, K., Yanai, H., Negishi, H., Asagiri, M., Sato, M., Mizutani, T., Shimada, N., Ohba, Y.,  
536 Takaoka, A., Yoshida, N., et al. (2005). IRF-7 is the master regulator of type-I interferon-dependent  
537 immune responses. *Nature* *434*, 772–777.

- 538 Iampietro, M., Aurine, N., Dhondt, K.P., Dumont, C., Pelissier, R., Spanier, J., Vallve, A., Raoul,  
539 H., Kalinke, U., and Horvat, B. (2020). Control of Nipah Virus Infection in Mice by the Host  
540 Adaptors Mitochondrial Antiviral Signaling Protein (MAVS) and Myeloid Differentiation Primary  
541 Response 88 (MyD88). *J Infect Dis* 221, S401–S406.
- 542 Ikegame, S., Takeda, M., Ohno, S., Nakatsu, Y., Nakanishi, Y., and Yanagi, Y. (2010). Both RIG-I  
543 and MDA5 RNA Helicases Contribute to the Induction of Alpha/Beta Interferon in Measles Virus-  
544 Infected Human Cells. *JVI* 84, 372–379.
- 545 Ishikawa, H., and Barber, G.N. (2008). STING is an endoplasmic reticulum adaptor that facilitates  
546 innate immune signalling. *Nature* 455, 674–678.
- 547 Ishikawa, H., Ma, Z., and Barber, G.N. (2009). STING regulates intracellular DNA-mediated, type I  
548 interferon-dependent innate immunity. *Nature* 461, 788–792.
- 549 Kranzusch, P.J., Lee, A.S.-Y., Berger, J.M., and Doudna, J.A. (2013). Structure of Human cGAS  
550 Reveals a Conserved Family of Second-Messenger Enzymes in Innate Immunity. *Cell Reports* 3,  
551 1362–1368.
- 552 Kranzusch, P.J., Lee, A.S.Y., Wilson, S.C., Solovykh, M.S., Vance, R.E., Berger, J.M., and  
553 Doudna, J.A. (2014). Structure-Guided Reprogramming of Human cGAS Dinucleotide Linkage  
554 Specificity. *Cell* 158, 1011–1021.
- 555 Liu, S., Cai, X., Wu, J., Cong, Q., Chen, X., Li, T., Du, F., Ren, J., Wu, Y.-T., Grishin, N.V., et al.  
556 (2015). Phosphorylation of innate immune adaptor proteins MAVS, STING, and TRIF induces  
557 IRF3 activation. *Science* 347, aaa2630–aaa2630.
- 558 Mankan, A.K., Schmidt, T., Chauhan, D., Goldeck, M., Höning, K., Gaidt, M., Kubarenko, A.V.,  
559 Andreeva, L., Hopfner, K., and Hornung, V. (2014). Cytosolic RNA:DNA hybrids activate the  
560 cGAS –STING axis. *EMBO J* 33, 2937–2946.
- 561 Mehand, M.S., Al-Shorbaji, F., Millett, P., and Murgue, B. (2018). The WHO R&D Blueprint: 2018  
562 review of emerging infectious diseases requiring urgent research and development efforts. *Antiviral*  
563 *Research* 159, 63–67.
- 564 Mogensen, T.H. (2009). Pathogen recognition and inflammatory signaling in innate immune  
565 defenses. *Clin Microbiol Rev* 22, 240–273, Table of Contents.
- 566 Mukai, K., Konno, H., Akiba, T., Uemura, T., Waguri, S., Kobayashi, T., Barber, G.N., Arai, H.,  
567 and Taguchi, T. (2016). Activation of STING requires palmitoylation at the Golgi. *Nat Commun* 7,  
568 11932.
- 569 Nanche, D., Varior-Krishnan, G., Cervoni, F., Wild, T.F., Rossi, B., Roubardin-Combe, C., and  
570 Gerlier, D. (1993). Human membrane cofactor protein (CD46) acts as a cellular receptor for  
571 measles virus. *J Virol* 67, 6025–32.
- 572 Neufeldt, C.J., Cerikan, B., Cortese, M., Frankish, J., Lee, J.-Y., Plociennikowska, A., Heigwer, F.,  
573 Joecks, S., Burkart, S.S., Zander, D.Y., et al. (2020). SARS-CoV-2 infection induces a pro-  
574 inflammatory cytokine response through cGAS-STING and NF-κB (Microbiology).  
575 <https://doi.org/10.1101/2020.07.21.212639>
- 576 Ni, G., Konno, H., and Barber, G.N. (2017). Ubiquitination of STING at lysine 224 controls IRF3  
577 activation. *Sci Immunol* 2.

- 578 Ni, G., Ma, Z., and Damania, B. (2018). cGAS and STING: At the intersection of DNA and RNA  
579 virus-sensing networks. *PLoS Pathog* 14, e1007148.
- 580 Noyce, R.S., Bondre, D.G., Ha, M.N., Lin, L.T., Sisson, G., Tsao, M.S., and Richardson, C.D.  
581 (2011). Tumor cell marker PVRL4 (nectin 4) is an epithelial cell receptor for measles virus. *PLoS*  
582 *Pathogens* 7, e1002240.
- 583 Park, A., and Iwasaki, A. (2020). Type I and Type III Interferons - Induction, Signaling, Evasion,  
584 and Application to Combat COVID-19. *Cell Host Microbe* 27, 870–878.
- 585 Pelissier, R., Iampietro, M., and Horvat, B. (2019). Recent advances in the understanding of Nipah  
586 virus immunopathogenesis and anti-viral approaches. *F1000Res* 8, 1763.
- 587 Runge, S., Sparrer, K.M.J., Lässig, C., Hembach, K., Baum, A., García-Sastre, A., Söding, J.,  
588 Conzelmann, K.-K., and Hopfner, K.-P. (2014). In Vivo Ligands of MDA5 and RIG-I in Measles  
589 Virus-Infected Cells. *PLoS Pathog* 10, e1004081.
- 590 Schoggins, J.W., MacDuff, D.A., Imanaka, N., Gainey, M.D., Shrestha, B., Eitson, J.L., Mar, K.B.,  
591 Richardson, R.B., Ratushny, A.V., Litvak, V., et al. (2014). Pan-viral specificity of IFN-induced  
592 genes reveals new roles for cGAS in innate immunity. *Nature* 505, 691–695.
- 593 Sen, G.C., and Peters, G.A. (2007). Viral stress-inducible genes. *Adv Virus Res* 70, 233–263.
- 594 Seth, R.B., Sun, L., Ea, C.-K., and Chen, Z.J. (2005). Identification and characterization of MAVS,  
595 a mitochondrial antiviral signaling protein that activates NF-kappaB and IRF 3. *Cell* 122, 669–682.
- 596 Shang, G., Zhu, D., Li, N., Zhang, J., Zhu, C., Lu, D., Liu, C., Yu, Q., Zhao, Y., Xu, S., et al.  
597 (2012). Crystal structures of STING protein reveal basis for recognition of cyclic di-GMP. *Nat*  
598 *Struct Mol Biol* 19, 725–727.
- 599 Sharma, K.B., Sharma, M., Aggarwal, S., Yadav, A.K., Bhatnagar, S., Vrati, S., and Kalia, M.  
600 (2019). Quantitative Proteome Analysis of *Atg5* -Deficient Mouse Embryonic Fibroblasts Reveals  
601 the Range of the Autophagy-Modulated Basal Cellular Proteome. *MSystems* 4, e00481-19,  
602 /msystems/4/6/msys.00481-19.atom.
- 603 Soman Pillai, V., Krishna, G., and Valiya Veetil, M. (2020). Nipah Virus: Past Outbreaks and  
604 Future Containment. *Viruses* 12.
- 605 Stempel, M., Chan, B., Juranić Lisnić, V., Krmpotić, A., Hartung, J., Paludan, S.R., Füllbrunn, N.,  
606 Lemmermann, N.A., and Brinkmann, M.M. (2019). The herpesviral antagonist m152 reveals  
607 differential activation of STING -dependent IRF and NF -κB signaling and STING 's dual role  
608 during MCMV infection. *EMBO J* 38.
- 609 Sun, B., Sundström, K.B., Chew, J.J., Bist, P., Gan, E.S., Tan, H.C., Goh, K.C., Chawla, T., Tang,  
610 C.K., and Ooi, E.E. (2017). Dengue virus activates cGAS through the release of mitochondrial  
611 DNA. *Sci Rep* 7, 3594.
- 612 Sun, L., Xing, Y., Chen, X., Zheng, Y., Yang, Y., Nichols, D.B., Clementz, M.A., Banach, B.S., Li,  
613 K., Baker, S.C., et al. (2012). Coronavirus Papain-like Proteases Negatively Regulate Antiviral  
614 Innate Immune Response through Disruption of STING-Mediated Signaling. *PLoS ONE* 7, e30802.
- 615 Sun, L., Wu, J., Du, F., Chen, X., and Chen, Z.J. (2013). Cyclic GMP-AMP synthase is a cytosolic  
616 DNA sensor that activates the type I interferon pathway. *Science* 339, 786–791.



- 617 Tanaka, Y., and Chen, Z.J. (2012). STING specifies IRF3 phosphorylation by TBK1 in the  
618 cytosolic DNA signaling pathway. *Sci Signal* 5, ra20.
- 619 Tatsuo, H., Ono, N., Tanaka, K., and Yanagi, Y. (2000). SLAM (CDw150) is a cellular receptor for  
620 measles virus. *Nature* 406, 893–897.
- 621 Tegtmeyer, P.-K., Spanier, J., Borst, K., Becker, J., Riedl, A., Hirche, C., Ghita, L., Skerra, J.,  
622 Baumann, K., Lienenklaus, S., et al. (2019). STING induces early IFN- $\beta$  in the liver and constrains  
623 myeloid cell-mediated dissemination of murine cytomegalovirus. *Nat Commun* 10, 2830.
- 624 Thibault, P.A., Watkinson, R.E., Moreira-Soto, A., Drexler, J.F., and Lee, B. (2017). Zoonotic  
625 Potential of Emerging Paramyxoviruses: Knowns and Unknowns. *Adv Virus Res* 98, 1–55.
- 626 Tsuchiya, Y., Jounai, N., Takeshita, F., Ishii, K.J., and Mizuguchi, K. (2016). Ligand-induced  
627 Ordering of the C-terminal Tail Primes STING for Phosphorylation by TBK1. *EBioMedicine* 9, 87–  
628 96.
- 629 Vincent, J., Adura, C., Gao, P., Luz, A., Lama, L., Asano, Y., Okamoto, R., Imaeda, T., Aida, J.,  
630 Rothamel, K., et al. (2017). Small molecule inhibition of cGAS reduces interferon expression in  
631 primary macrophages from autoimmune mice. *Nat Commun* 8, 750.
- 632 Wathélet, M.G., Lin, C.H., Parekh, B.S., Ronco, L.V., Howley, P.M., and Maniatis, T. (1998).  
633 Virus Infection Induces the Assembly of Coordinately Activated Transcription Factors on the IFN- $\beta$   
634 Enhancer In Vivo. *Molecular Cell* 1, 507–518.
- 635 Wesche, H., Henzel, W.J., Shillinglaw, W., Li, S., and Cao, Z. (1997). MyD88: an adapter that  
636 recruits IRAK to the IL-1 receptor complex. *Immunity* 7, 837–847.
- 637 Xie, W., Lama, L., Adura, C., Tomita, D., Glickman, J.F., Tuschl, T., and Patel, D.J. (2019).  
638 Human cGAS catalytic domain has an additional DNA-binding interface that enhances enzymatic  
639 activity and liquid-phase condensation. *Proc Natl Acad Sci U S A* 116, 11946–11955.
- 640 Yamamoto, M., Sato, S., Hemmi, H., Hoshino, K., Kaisho, T., Sanjo, H., Takeuchi, O., Sugiyama,  
641 M., Okabe, M., Takeda, K., et al. (2003). Role of adaptor TRIF in the MyD88-independent toll-like  
642 receptor signaling pathway. *Science* 301, 640–643.
- 643 Yeow, W.-S., Au, W.-C., Juang, Y.-T., Fields, C.D., Dent, C.L., Gewert, D.R., and Pitha, P.M.  
644 (2000). Reconstitution of Virus-mediated Expression of Interferon  $\alpha$  Genes in Human Fibroblast  
645 Cells by Ectopic Interferon Regulatory Factor-7. *J. Biol. Chem.* 275, 6313–6320.
- 646 Zevini, A., Olganier, D., and Hiscott, J. (2017). Crosstalk between Cytoplasmic RIG-I and STING  
647 Sensing Pathways. *Trends in Immunology* 38, 194–205.
- 648 Zhang, X., Wu, J., Du, F., Xu, H., Sun, L., Chen, Z., Brautigam, C.A., Zhang, X., and Chen, Z.J.  
649 (2014). The Cytosolic DNA Sensor cGAS Forms an Oligomeric Complex with DNA and  
650 Undergoes Switch-like Conformational Changes in the Activation Loop. *Cell Reports* 6, 421–430.
- 651 Zhong, B., Yang, Y., Li, S., Wang, Y.-Y., Li, Y., Diao, F., Lei, C., He, X., Zhang, L., Tien, P., et al.  
652 (2008). The adaptor protein MITA links virus-sensing receptors to IRF3 transcription factor  
653 activation. *Immunity* 29, 538–550.
- 654